

CrossMark
click for updates

Cite this: DOI: 10.1039/c4cy01126k

Biogas dry reforming for syngas production: catalytic performance of nickel supported on waste-derived SiO₂^{†‡}

Xuejing Chen,^a Jianguo Jiang,^{*abc} Sicong Tian^a and Kaimin Li^a

SiO₂ synthesized from photovoltaic waste by a vapor-phase hydrolysis method was applied as a support for a nickel catalyst in a biogas dry reforming process for the first time. The catalytic performance was compared with those of commercial precipitated SiO₂ and ordered mesoporous SiO₂. Nickel supported on waste-derived SiO₂ exhibited high CH₄ conversion (92.3%) and high CO₂ conversion (95.8%) at 800 °C, and there was no deactivation after a 40 h-on-stream test. Catalyst characterization results revealed that the S_{BET} values and pore properties of catalysts affected the catalytic performance. A higher pore volume/S_{BET} ratio led to a smaller crystal metal size and higher metal dispersion, thus the catalyst was less prone to deactivation. This discovery will help improve catalyst design. The use of nickel supported on waste-derived SiO₂, which is competitive with commercial and mesoporous catalysts, shows the use of photovoltaic waste as a high value-added product; it can also deliver a cheap and environmentally benign support for catalysts in the biogas dry reforming process.

Received 30th August 2014,
Accepted 23rd September 2014

DOI: 10.1039/c4cy01126k

www.rsc.org/catalysis

1. Introduction

Biogas is a mixture of mainly methane and carbon dioxide, which is produced by the anaerobic digestion of residual biomass, such as landfill waste, municipal sludge, and food waste. With the growing concern regarding global climate change due to anthropogenic CO₂ emission, biogas recycling for energy-related applications has received much attention.¹ Therefore, biogas dry reforming for syngas production (eqn (1)) is a recycling option with several advantages: (i) biogas dry reforming process can simultaneously consume the two main greenhouse gases (CH₄ and CO₂); (ii) the H₂/CO ratio is close to 1, which makes it suitable for further use in the carbonylation, hydroformylation, and Fischer–Tropsch synthesis of long-chain hydrocarbons;² and (iii) the process avoids the separation of CO₂, which is an energy intensive and costly process.^{3–5}



The high cost and energy consumption of biogas dry reforming have restricted its industrial application.⁶ Because

biogas dry reforming is a strongly endothermic process (see eqn (1)), the high reaction temperature will achieve a relatively high conversion of reactants.^{7,8} In addition, catalysts also play a vital role in the catalytic dry reforming process, which increases the cost substantially. Improving the stability and choosing relatively cheap raw materials to prepare the catalyst, without a loss of catalyst activity, are important.

The main obstacle to improve stability is the deactivation of catalysts, which is caused mainly by the deposition of inactive carbon and the sintering of active metals.^{9,10} To improve catalyst stability, many studies have been conducted, optimizing the active metals, catalyst supports, and catalyst preparation methods.^{3,11–14} During these processes, the low cost and availability of the raw materials used for catalyst preparation are important. Ni-based catalysts are commonly used in the dry reforming process due to their reasonably good activity and low cost compared to noble metals, although they are more sensitive to coke formation than the noble metals.^{2,10,13,15} Many dioxides including SiO₂,^{12,16–18} ZrO₂,¹⁹ MgO,²⁰ TiO₂,⁸ CeO₂,¹¹ Al₂O₃,^{3,21} and their hybrids^{15,22,23} have been used as catalyst supports in the reforming process due to their high specific surface areas and high thermal stability. Among these, SiO₂ and SiO₂-based catalyst supports are the most widely used and the most promising for the industrial application of the dry reforming process due to their availability and various phase morphologies. Frontera *et al.*¹² investigated the activity and stability of several nickel catalysts supported on different types of highly crystalline silica zeolites, including Ni-ITQ-6, Ni-silicalite-1, and Ni-MCM-41, and found

^a School of Environment, Tsinghua University, Beijing 100084, China.

E-mail: jianguoj@mail.tsinghua.edu.cn; Fax: +86 10 62783548;

Tel: +86 10 62783548

^b Key Laboratory for Solid Waste Management and Environment Safety, Ministry of Education of China, China^c Collaborative Innovation Center for Regional Environmental Quality, China

† The authors declare no competing financial interest.

‡ Electronic supplementary information (ESI) available. See DOI: 10.1039/c4cy01126k

that the heterogeneity of the support surface strongly affected the catalyst performance. Ning Wang *et al.*¹⁸ also found that the pore topology of different types of SiO₂ affected the particle dispersion, reducibility, and catalytic behavior of catalysts. The synthesis of silica zeolites consumes large amounts of organic template agents, and these zeolites are currently not commercially available in large quantities.²⁴ Therefore, the development of new silica materials with a high specific surface area, high thermal stability, and most importantly, the potential for large-scale production is essential.

In our previous study, polyporous nano-silica synthesized from photovoltaic waste SiCl₄ using a low-temperature vapor-phase hydrolysis method (designated as SiO₂-H) was shown to have a relatively high specific surface area and high thermal stability.²⁵ Considering the large-scale production and poor treatment conditions of photovoltaic waste SiCl₄, the production of SiO₂-H as well as its further application as a catalyst support for biogas dry reforming represents a useful conversion of photovoltaic waste to a high value-added product; it also provides a cheap and environmentally benign support for catalysts in the biogas dry reforming process. Using SiO₂-H as a waste-derived SiO₂ support in biogas catalytic dry reforming applications has not been reported previously.

A comprehensive evaluation of the catalytic performance of nickel supported on waste-derived SiO₂ in biogas dry reforming was undertaken. SiO₂-H was used as a support for a nickel catalyst in a biogas dry reforming process for the first time, and commercial precipitated SiO₂ and mesoporous SiO₂ were also considered for comparison. Catalytic tests of the three different nickel supported catalysts and the related characterization of both fresh and spent catalysts were undertaken systematically.

2. Materials & methods

2.1 Support and catalyst preparation

A low-temperature vapor-phase hydrolysis method was used to synthesize SiO₂-H as previously reported.²⁵ Silicon tetrachloride (99%, LDK Solar Ltd., Xinyu, China) was vaporized and hydrolyzed with water vapor at a temperature of 200 °C, a retention time of 5 s, and a H₂O/SiCl₄ molar ratio of 2. Silica powder was collected and dried at 105 °C for 2 h.

Commercial precipitated SiO₂ (designated as SiO₂-P) and ordered mesoporous silica (SBA-15) were purchased (Sigma-Aldrich, St. Louis, MO, USA). All three SiO₂ supports were calcined at 700 °C for 4 h to enhance their thermal stability and remove surface moisture.

An ultrasonic-assisted wetness impregnation method was used to prepare Ni/SiO₂ catalysts with 10 wt% Ni. The metallic precursor solution was obtained by dissolving Ni(NO₃)₂·6H₂O (99%, Sigma-Aldrich) in ethanol with a Ni/ethanol ratio of 2 g L⁻¹. The three SiO₂ supports were dispersed in ethanol after ultrasonic oscillation to obtain a SiO₂ colloidal solution. The Ni precursor solution was then added dropwise to the SiO₂ colloidal solution under magnetic stirring. The solution was agitated at 70 °C for 12 h to remove the ethanol.

The catalysts were dried at 60 °C for 6 h in a vacuum oven and calcined at 800 °C for 4 h. Catalysts synthesized from the SiO₂-H, SBA-15, and the SiO₂-P supports were designated Ni/SiO₂-H, Ni/SBA-15, and Ni/SiO₂-P, respectively.

2.2 Catalyst characterization

XRD patterns were obtained with a D8 Advance X-ray diffractometer (Siemens, Munich) using Cu K α radiation ($\lambda = 0.15406$ nm), with a 2θ range of 0.3–80°. Scherrer's equation was used to estimate the mean Ni crystallite size based on the diffraction peaks of the Ni (200) facet. Analysis of the Ni loading of catalysts was undertaken using an XRF analyzer (XRF-1800, Shimadzu).

Textual properties were measured by a surface area and porosity analyzer (ASAP 2020 HD88, Micromeritics) through the nitrogen adsorption-desorption isotherms at 77 K. The samples were degassed at 90 °C for 60 min and held at 160 °C for 120 min before analysis. A Brunauer-Emmett-Teller (BET) model was used to calculate the specific surface area and a Barrett-Joyner-Halenda (BJH) model was used to calculate the pore volume distribution.

Transmission electron microscopy (TEM) (JEM-2011, JEOL Ltd.) was used to observe the morphology and distribution of metal sites. The samples were first dispersed in ethanol, and then one drop of ethanol solution was placed on a copper grid pre-coated with a formvar film and dried in air. SEM (S-5500, Hitachi) was also used to observe the morphology of the samples.

The H₂ temperature-programmed reduction (H₂-TPR) was employed to analyze the reduction behavior of catalysts using a chemisorption analyzer (AutoChemII 2920, Micromeritics). Catalyst samples (50 mg, 20–40 mesh) were pretreated at 400 °C for 1 h under flowing Ar (30 ml min⁻¹). Upon cooling to 50 °C, the sample was heated from room temperature (RT) to 1000 °C with a temperature ramp of 10 °C min⁻¹ under a 5 vol% H₂/Ar stream (50 mL min⁻¹).

The TGA-MS method was applied to investigate the carbon deposition with a TGA/DSC 1 STARE system (Mettler Toledo) and a ThermoStar mass spectrometer (Pfeiffer). Samples were treated at a rate of 10 °C min⁻¹ from RT to 900 °C under an oxygen stream of 20 mL min⁻¹ with nitrogen as a protection gas.

2.3 Catalytic tests

Catalytic tests for biogas dry reforming were conducted in a fixed-bed reactor with a quartz glass tube (diameter = 6 mm) under atmospheric pressure. 200 mg of the samples (20–40 mesh) were loaded in the center of the tube reactor. Before the test, the catalysts were reduced at 800 °C *in situ* for 1 h under a flow of 10 vol% H₂/N₂. A mixture gas (CH₄ : CO₂ : N₂ = 0.4 : 0.4 : 0.2) with a flow rate of 50 mL min⁻¹ was used, in which N₂ was the reference gas for end gas analysis. The products were analyzed using on-line GC apparatus (GC-2014, Shimadzu) with a combined PC-1, MC-1, and MC-2 chromatographic column and a thermal conductivity detector. Catalytic activity of all of the samples, including a blank

sample (20–40 mesh SiO₂ support without Ni), was tested at temperatures from 600 to 900 °C after being in a steady state for 1 h. Stability tests of Ni/SiO₂-H, Ni/SBA-15, and Ni/SiO₂-P were conducted at 800 °C for 40 h on-stream, and the products were analyzed every 30 min. The conversion (*X*) and the H₂/CO ratio were calculated as follows:

$$X_{\text{CH}_4} (\%) = \frac{[\text{CH}_4]_{\text{in}} - [\text{CH}_4]_{\text{out}}}{[\text{CH}_4]_{\text{in}}} \times 100$$

$$X_{\text{CO}_2} (\%) = \frac{[\text{CO}_2]_{\text{in}} - [\text{CO}_2]_{\text{out}}}{[\text{CO}_2]_{\text{in}}} \times 100$$

$$\frac{\text{H}_2}{\text{CO}} \text{ ratio} = \frac{\text{moles of H}_2 \text{ produced}}{\text{moles of CO produced}}$$

3 Results and discussion

3.1 Characterization of fresh catalysts

The XRD patterns of fresh catalysts are shown in Fig. 1. Reflections of SiO₂ and NiO were detected in the wide-angle XRD patterns of all three fresh SiO₂-supported nickel catalysts (Fig. 1a). Three sharp peaks were clearly visible at 37.3°, 43.3° and 62.9°, which corresponded to the (111), (200), and (220) reflections of the crystal NiO structure, respectively (PDF#47-1049). Strong and broad diffractions with a wide 2θ range at 15–30° were assigned to amorphous SiO₂.²⁶ Compared to Ni/SiO₂-H and Ni/SiO₂-P, Ni/SBA-15 had a less erratic diffraction peak at 15–30°. This may be because SBA-15 has a highly ordered mesoporous structure. This was confirmed by the small-angle XRD patterns (Fig. 1b). Ni/SBA-15 had remarkable peaks of ordered mesoporous silica (100), (110), and (200) planes, indicating a high degree of hexagonal mesoscopic organization.^{27,28} No peaks were found in the small-angle XRD patterns of Ni/SiO₂-H and Ni/SiO₂-P, indicating heterogeneous porosity.

The average crystallite size of NiO was determined by the diffraction peak of the NiO (200) plane in the XRD patterns, using Scherrer's equation (Table 1). The average crystal metal size increased in the order Ni/SiO₂-P < Ni/SiO₂-H < Ni/SBA-15, indicating a decreasing Ni dispersion order Ni/SiO₂-P > Ni/SiO₂-H > Ni/SBA-15.^{26,29} The BET specific surface area (*S*_{BET}) value and pore properties of catalyst supports and freshly prepared catalysts are shown in Table S1.† After impregnation, the *S*_{BET} value and pore volume decreased for the three catalysts. This phenomenon might be caused by pore blocking during the impregnation process. The *S*_{BET}, pore volume, average pore size, and average Ni loading of freshly prepared catalysts are also presented in Table 1. The largest pore volume and largest average pore size were found in Ni/SiO₂-P, while Ni/SBA-15 had the largest *S*_{BET} value. There was no obvious connection between the *S*_{BET} value and the pore volume of the catalysts, but the pore volume/*S*_{BET} ratio decreased in the order Ni/SiO₂-P > Ni/SiO₂-H > Ni/SBA-15, which was in accordance

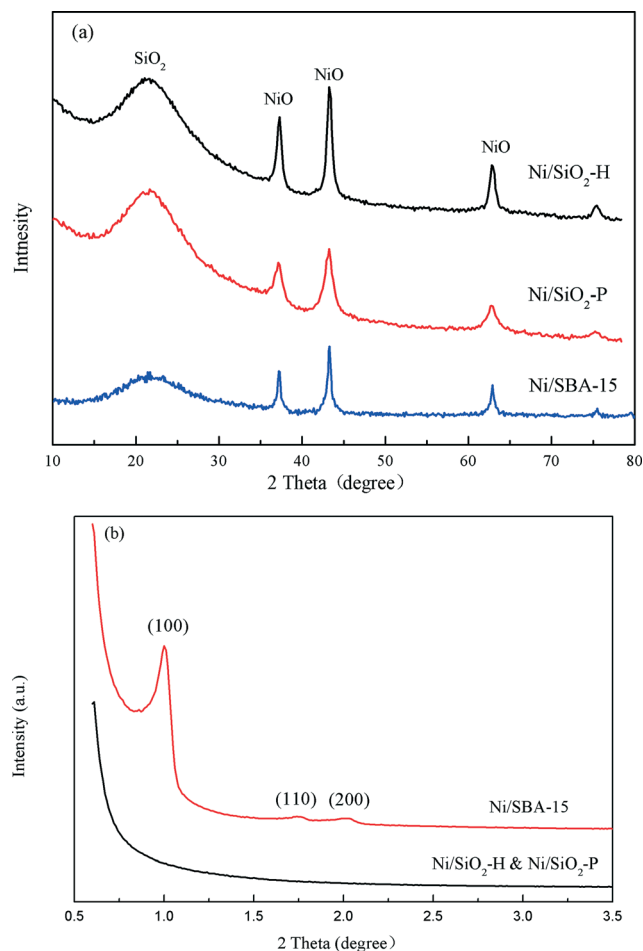


Fig. 1 XRD patterns of fresh 10% Ni/SiO₂ catalysts (before reduction): (a) wide-angle XRD patterns and (b) small-angle XRD patterns.

with the Ni dispersion order. Bappy Saha³⁰ also proved that a high pore volume/*S*_{BET} ratio contributes to high catalytic performance. The XRF results in Table 1 show that the Ni loading was slightly higher than the set value of 10 wt%. This might be caused by the weight loss during the pre-calcination of the supports, resulting in a higher Ni content in the catalysts.

SEM images of the three supports are shown in Fig. S1.† From the SEM images of the supports, we can see that both SiO₂-H and SiO₂-P have a loose and porous structure with a non-uniform pore size, while SBA-15 has uniform cylindrical pores. TEM images of fresh catalysts are shown in Fig. 2. The translucent particles with an irregular shape are the supports of Ni/SiO₂-H and Ni/SiO₂-P catalysts (Fig. 2a and b);²⁵ the crystal NiO particles were uniformly supported on SiO₂-H and SiO₂-P. In contrast, Ni/SiO₂-P had a smaller NiO particle size and greater homogeneity of metal dispersion. In Fig. 2c and d, a two-dimensional hexagonal texture is observed in SBA-15.^{15,31} The pores of Ni/SBA-15 exhibited a uniform size of ~5 nm (Fig. S2.†), which is also confirmed by the BET results in Table 1. Some NiO particles were uniformly loaded on the outside surface of SBA-15, which differed greatly from the crystallite sites inside the porous structure. The regulated growth of crystals inside the narrowly distributed channels

Table 1 Main textural properties of fresh catalysts

Catalysts	Ni loading ^a wt. (%)	Average crystal size ^b nm	S_{BET}^c $\text{m}^2 \text{g}^{-1}$	Pore volume $\text{cm}^3 \text{g}^{-1}$	Average pore size \AA	Pore volume to S_{BET} ratio 10^{-9} m
Ni/SiO ₂ -H	10.55	8.38	153	0.40	107	2.6
Ni/SBA-15	10.90	10.23	332	0.42	50	1.3
Ni/SiO ₂ -P	10.15	6.25	279	0.88	126	3.2

^a Determined by the XRF method. ^b Determined using Scherrer's equation from the diffraction of the Ni (200) plane. ^c Specific surface area calculated by the BET method.

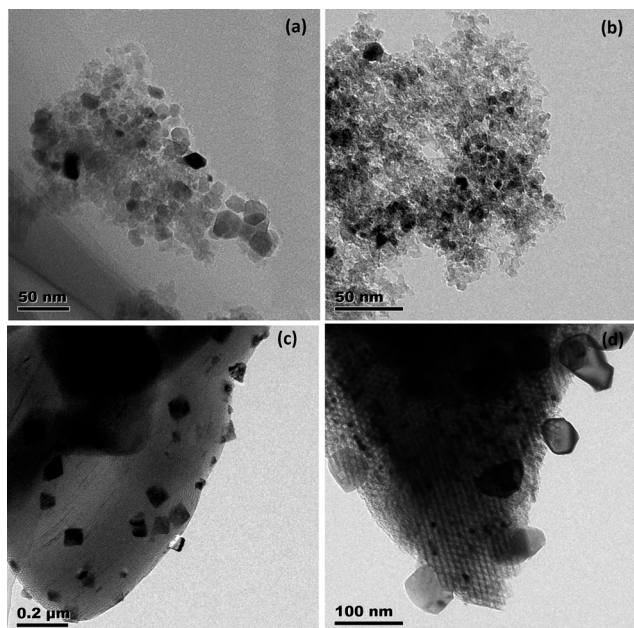


Fig. 2 TEM images of fresh catalysts (before reduction): (a) Ni/SiO₂-H, (b) Ni/SiO₂-P, (c) and (d) Ni/SBA-15.

might have been responsible for the difference in the NiO particle size, resulting in less homogeneity of NiO particles than those in Ni/SiO₂-P and Ni/SiO₂-H. The particle size of supported NiO increased in the order Ni/SiO₂-P < Ni/SiO₂-H < Ni/SBA-15, which was in agreement with the results from Scherrer's equation.

The reducibility and different Ni species in the SiO₂-supported nickel catalysts were investigated using H₂-TPR (Fig. 3). All of the catalysts had a broad and overlapping H₂ consumption peak from 300 to 800 °C, indicating the presence of nickel oxides that had different interactions with the supports.^{16,32} The highest H₂ reduction temperature of Ni/SiO₂-H, Ni/SBA-15, and Ni/SiO₂-P was 680 °C, 700 °C, and 750 °C, respectively, in the order Ni/SiO₂-H < Ni/SBA-15 < Ni/SiO₂-P, suggesting an enhancement of NiO–SiO interactions.^{26,33} In addition, two separate reduction regions can be seen in the Ni/SBA-15 catalyst, *i.e.*, the broad peak at 430 °C and the shoulder peak around 620 °C. These peaks might be related to the reduction of NiO particles supported on the outside surface and those inside the porous structure of SBA-15, respectively, which can also be clearly distinguished

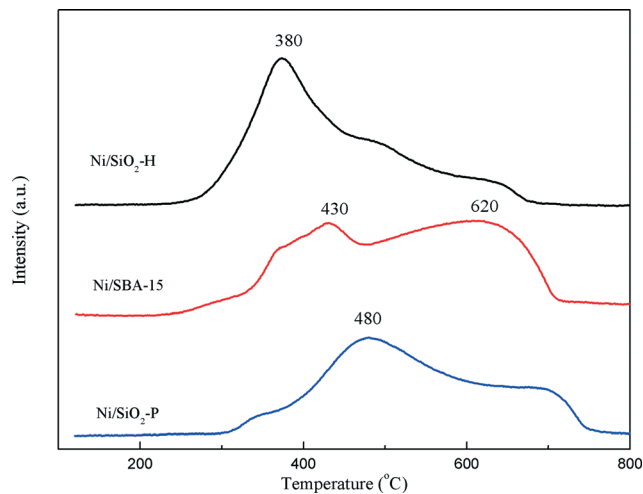


Fig. 3 H₂-TPR profiles of Ni/SiO₂ catalysts (reduced under a 5 vol% H₂/Ar stream at a temperature ramp of 10 °C min⁻¹).

in the TEM results. The H₂-TPR profiles also confirmed that 800 °C was the appropriate pre-reduction temperature for the reduction of reducible catalysts.

3.2 Catalytic performance in biogas reforming

Effect of temperature. The dry reforming activity of catalysts is indicated by the conversion of CH₄ and CO₂, and the selectivity is expressed in terms of the H₂/CO ratio. Fig. 4 shows the activity and selectivity results for all the three types of SiO₂-supported nickel catalysts from 600 to 900 °C. Generally, the conversion of both CH₄ and CO₂ increased as the temperature increased from 600 to 900 °C. This may be because the dry reforming reaction of biogas is a strongly endothermic reaction (eqn (1)), and a higher temperature will increase the conversion rate, as observed in earlier studies.^{6,7,34} Among the different catalysts, the CH₄ conversion of Ni/SiO₂-H was the highest for the whole temperature range, and when the temperature was higher than 650 °C, the CH₄ conversion of Ni/SiO₂-P was slightly higher than that of Ni/SBA-15. As the temperature increased, less difference was observed in the CO₂ conversion of the different catalysts. Taking Ni/SiO₂-H as an example, the CH₄ conversion increased from 55% to 98% and the CO₂ conversion increased from 52% to 98% when the temperature increased from 600 to 900 °C. When the temperature was

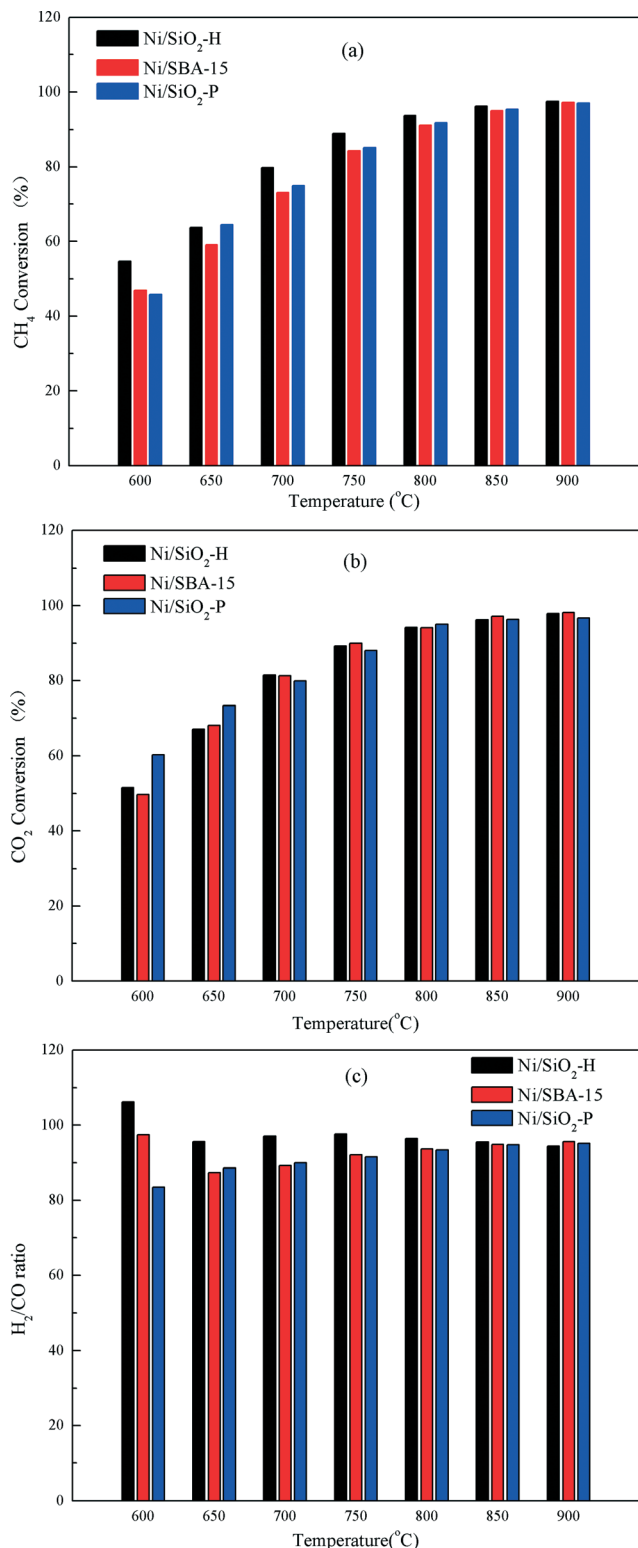
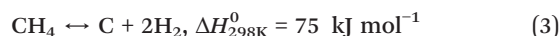
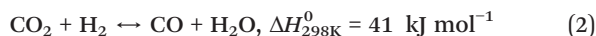


Fig. 4 The influence of temperature on the catalytic activity of Ni/SiO₂ catalysts: (a) CH₄ conversion, (b) CO₂ conversion, and (c) H₂/CO ratio (GHSV = 15 000 mL g_{cat}⁻¹ h⁻¹, atmospheric pressure).

800 °C, both CH₄ and CO₂ conversions exceeded 90%. There is only a slight increase in CH₄ and CO₂ conversions at temperatures >800 °C.

The H₂/CO ratio of the different catalysts at various temperatures is shown in Fig. 4c. When the temperature was higher than 650 °C, the H₂/CO ratio of all samples was <1. The reverse water-gas shift reaction (RWGS, eqn (2)) can consume the additional H₂ and produce CO, which lowers the H₂/CO ratio.⁹ When the temperature was <850 °C, the H₂/CO ratio of Ni/SiO₂-H was slightly higher than those of Ni/SBA-15 and Ni/SiO₂-P, indicating a smaller contribution from the RWGS reaction.



Stability tests. Temperature tests indicated that at 800 °C, both CH₄ and CO₂ conversions were high (>90%). Blank tests showed that when the temperature was higher than 750 °C, H₂ and CO were detected in the outlet gas (Fig. S3[†]), which might be caused by RWGS reaction (eqn (2)) and methane decomposition reaction (eqn (3)). Therefore, 800 °C was chosen as the appropriate temperature to conduct stability tests. Fig. 5 shows the 40 h on-stream catalyst test results for all catalyst samples at 800 °C. All three of the samples showed good stability during the 40 h on-stream, and no decay of activity was found in all samples. The conversion of CH₄ was slightly lower than the conversion of CO₂ and the H₂/CO ratio was <1.

The average CH₄ conversion, CO₂ conversion, and H₂/CO ratio are summarized in Table 2. The average CH₄ conversion increased in the order Ni/SBA-15 < Ni/SiO₂-P < Ni/SiO₂-H, and the average CO₂ conversion increased in the order Ni/SBA-15 < Ni/SiO₂-H < Ni/SiO₂-P. The contribution of the RWGS reaction increased the conversion of CO₂ and decreased the H₂/CO ratio. The higher the degree of the reverse water-gas shift reaction process, the larger the difference between CH₄ and CO₂ conversion and the lower the H₂/CO ratio. These theoretical considerations are confirmed by the actual test results shown in Table 2. The highest average H₂/CO ratio of Ni/SiO₂-H indicated that the secondary reaction was minimized to a greater extent than in Ni/SBA-15 and Ni/SiO₂-P.

3.3 Post-reaction characterization

Fig. 6 shows the N₂ adsorption–desorption isotherms and BJH desorption pore size distribution analysis of fresh and spent catalysts. The N₂ adsorption–desorption isotherms of both fresh and spent Ni/SiO₂-H (Fig. 6a) and Ni/SiO₂-P (Fig. 6c) catalysts displayed an approximate type IV isotherm, as defined by the International Union of Pure and Applied Chemistry (IUPAC). The presence of a H3-type hysteresis loop indicates the existence of mesopores, and the unlimited adsorption at high P/P₀ values suggests that aggregates of plate-like particles give rise to slit-shaped pores.^{24,35} The results were also confirmed by Fig. 2a and b. The N₂

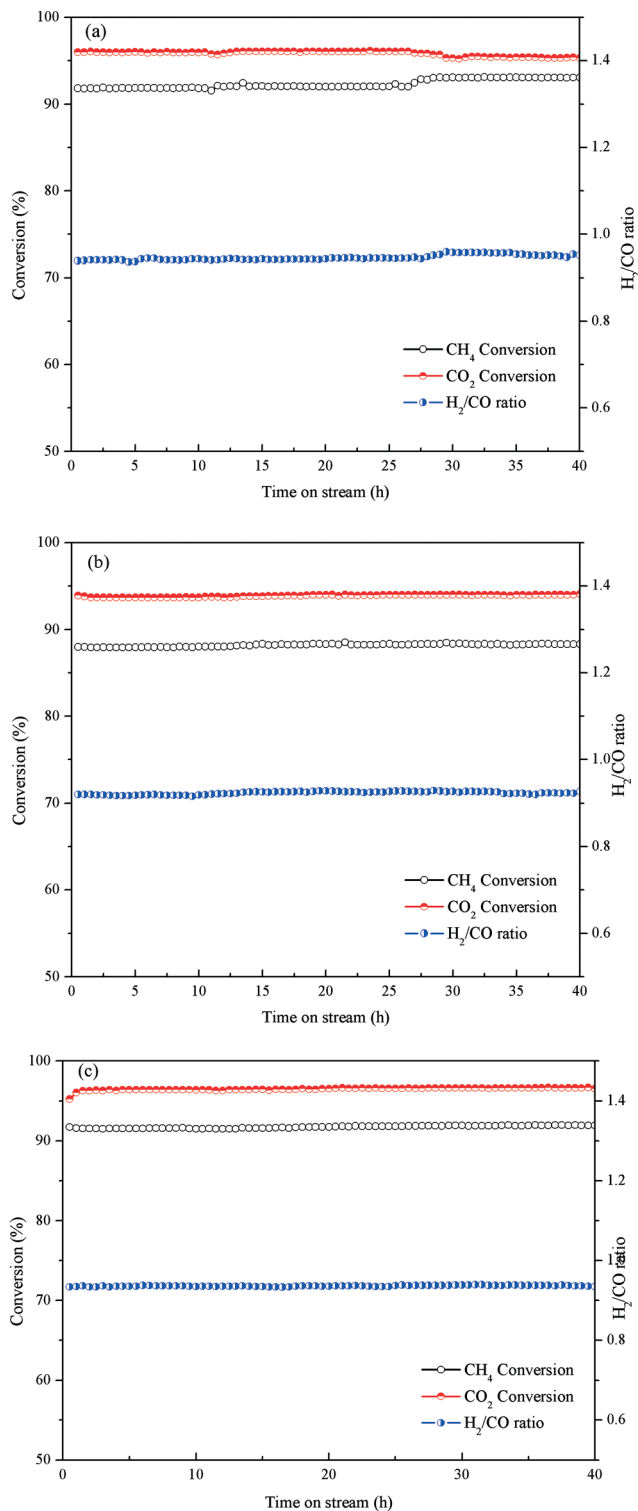


Fig. 5 Stability tests of Ni/SiO₂ catalysts at 800 °C for 40 h: (a) Ni/SiO₂-H, (b) Ni/SBA-15, and (c) Ni/SiO₂-P (GHSV = 15 000 mL g_{cat}⁻¹ h⁻¹, atmospheric pressure).

adsorption-desorption isotherms of both fresh and spent Ni/SBA-15 (Fig. 6b) catalysts displayed a typical type IV isotherm and a standard H1-type hysteresis loop, as defined by the IUPAC, and were characteristic of mesoporous materials

Table 2 Average catalytic activity of the three catalyst samples during the 40 h on-stream test

Catalysts	Average CH ₄ conversion (%)	Average CO ₂ conversion (%)	Conversion difference (%)	Average H ₂ /CO ratio
Ni/SiO ₂ -H	92.3	95.8	3.5	0.946
Ni/SBA-15	88.2	93.9	5.7	0.924
Ni/SiO ₂ -P	91.8	96.5	4.7	0.937

with highly uniform cylindrical pores,²⁷ which also supports the XRD and TEM results. The fresh Ni/SiO₂-H and Ni/SiO₂-P catalysts had a wide BJH desorption pore size distribution, while fresh Ni/SBA-15 had a highly narrow size distribution with a mean diameter of 5.0 nm, which was in accordance with the HR-TEM results (Fig. S2†).

After the 40 h on-stream tests, there was a decrease in the BET surface area and pore volume and an increase in the average pore size of all the spent catalysts (see Table S1†). This agreed with the BET analysis results for Ni/γ-Al₂O₃ reported by Srinivas Appari.³⁶ The catalytic reaction process did not change the shape of the N₂ adsorption-desorption isotherms of Ni/SiO₂-H and Ni/SBA-15, or their BJH desorption pore size distributions, and only a slight change in the average pore size was observed due to a slight blocking phenomenon. There was a difference in the hysteresis loops of the fresh and spent Ni/SiO₂-P catalysts. The shift in the relative pressure of the hysteresis loop to a higher value was observed, leading to an obvious change in the BJH desorption pore size distribution, with the average pore size shifted greatly from 126 to 270 nm. According to Aziz,²⁷ the hysteresis loops at lower and higher relative pressures represent the intra- and interparticle porosity, respectively. There might be a decrease in intraparticle porosity and an increase in the interparticle porosity of Ni/SiO₂-P after a stability test, therefore the decrease in pore volume due to intraparticle porosity may result in an increase of the average pore size.

Fig. 7 shows TEM images of spent catalysts. The original structure of all catalysts was maintained after 40 h on-stream tests. Spent Ni/SiO₂-H and Ni/SiO₂-P catalysts kept their amorphous structures, and Ni/SBA-15 kept its two-dimensional hexagonal texture. However, there was an obvious pore size increase in the spent Ni/SiO₂-P catalyst (Fig. 7b), which was supported by the BJH pore size distribution results shown in Fig. 6c. A slight metal agglomeration phenomenon was observed in spent Ni/SiO₂-H and Ni/SiO₂-P catalysts (Fig. 7a and b). The two-dimensional hexagonal channel of spent Ni/SBA-15 limited the agglomeration of active metals inside the pore (Fig. 7c), while the active metals supported on the outside surface experienced significant agglomeration, even those detached from the SBA-15 support (Fig. 7d). Ilenia Rossetti *et al.* also reported that large particles exposed a small interface with the support surface, which led to a weaker interaction, thus easy detachment from the support.²⁶ No carbon was found in any of the three spent catalysts, indicating negligible coke deposition.

The results of the TGA-MS analysis of the spent catalysts are shown in Fig. 8. The thermograms can be divided into

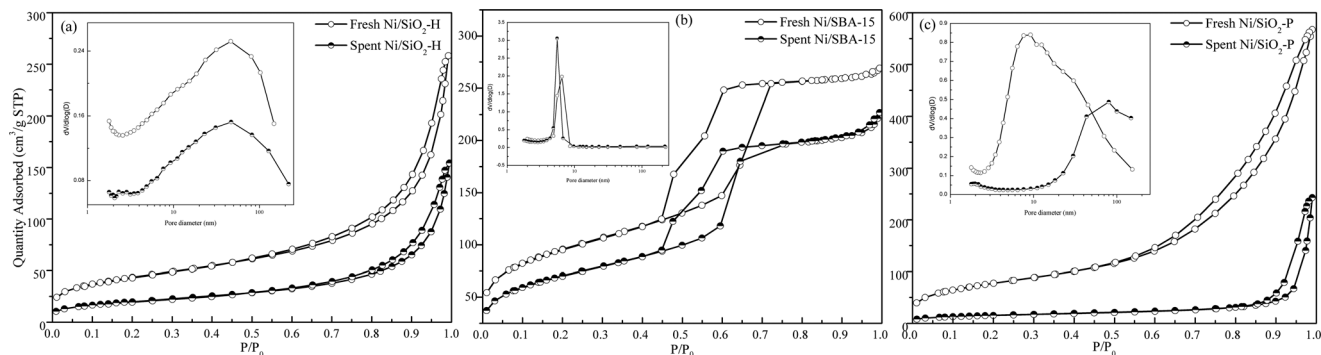


Fig. 6 N_2 adsorption-desorption isotherms and the BJH desorption pore size distributions of fresh and spent catalysts: (a) Ni/SiO₂-H, (b) Ni/SBA-15, and (c) Ni/SiO₂-P. The inset shows the pore size distribution.

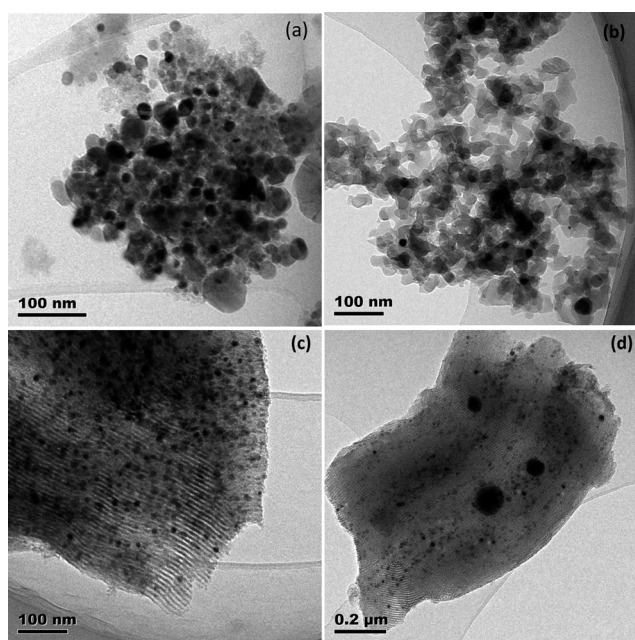


Fig. 7 TEM images of spent catalysts: (a) Ni/SiO₂-H, (b) Ni/SiO₂-P, and (c and d) Ni/SBA-15.

two different temperature regions (Fig. 8a). All of the spent catalysts experienced an increase in weight at low temperature ranges and a decrease in weight at high temperature ranges. The oxidation of nickel particles at temperatures above 200 °C caused the weight increase, and the 3% weight increase of the spent catalysts was inconsistent with the theoretical weight increase of 10% due to nickel particle oxidation, which was also reported by Jianqiang Zhu.¹⁷ Weight loss at temperatures above 400 °C was ascribed to the oxidation of deposited carbon.³⁷ CO₂ MS signals from the TPO process of the three spent catalysts are shown in Fig. 8b. Since O₂ was used as a reaction gas and N₂ was used as a protection gas, the signal for a molecular weight of 44 was only supposed to be CO₂, which was generated by the oxidation of deposited carbon. The CO₂ generation peak range of spent Ni/SiO₂-H, Ni/SBA-15, and Ni/SiO₂-P was 450–700 °C, 500–700 °C, and 580–700 °C, respectively, corresponding to the weight loss temperature ranges of the three catalysts. Although MS is a semi-quantitative method,

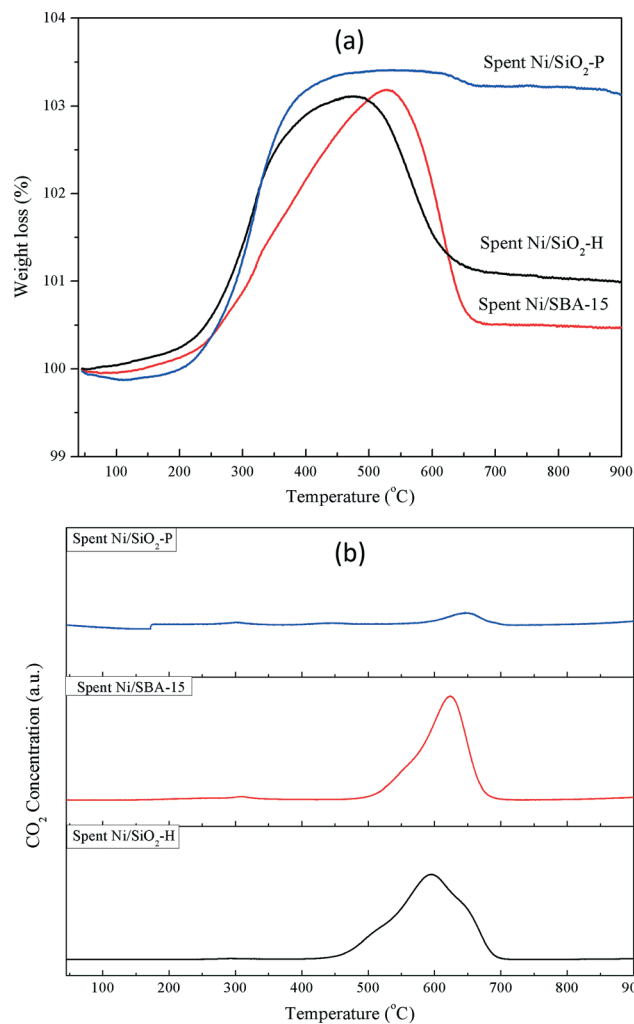


Fig. 8 (a) TGA profiles of spent Ni/SiO₂ catalysts. (b) MS signals of CO₂ (20 mL min⁻¹ O₂ stream at a temperature ramp of 10 °C min⁻¹ with N₂ as a protection gas).

we can still distinguish that a higher amount of weight loss from TGA resulted in a higher MS signal intensity. Thus, the very weak CO₂ signal intensity of spent Ni/SiO₂-P implied that it has the lowest carbon deposit. The amount of coke deposited on spent Ni/SiO₂-H, Ni/SBA-15, and Ni/SiO₂-P catalysts was calculated to be 2.1, 2.7, and 0.3 wt.%, respectively, which was

in the low range of carbon deposited (0.89–6.56 wt.%) on Ni/SiO₂ catalysts after a 30 h test, as reported by Zhu.¹⁷ In conclusion, the results showed that little coke was deposited on the catalysts, and the formation of coke was related to the metal dispersion of the catalysts. The smaller crystal size of metal catalysts will lead to a catalyst that is less prone to deactivation.

4 Conclusions

In summary, waste-derived SiO₂ obtained from photovoltaic waste SiCl₄ by a vapor-phase hydrolysis method was applied as the support for a nickel catalyst in a biogas dry reforming process for the first time. Catalytic test results showed that the conversion of CH₄ and CO₂ increased as temperature increased from 600 to 900 °C. When the temperature was 800 °C, it reached a high CH₄ conversion (92.3%) and a high CO₂ conversion (95.8%), and there was no deactivation after the 40 h on-stream test. Comparison with commercial precipitated SiO₂ and ordered mesoporous SiO₂ showed that the catalytic activity of waste-derived SiO₂ is equivalent to that of commercial precipitated SiO₂ and even superior to that of mesoporous SiO₂. The amount of coke deposited after stability tests follows the order commercial precipitated SiO₂ < waste-derived SiO₂ < mesoporous SiO₂. It is further demonstrated that coke deposition in the biogas dry reforming process is related to the textural properties of catalysts. A higher pore volume/S_{BET} ratio will lead to a smaller crystal metal size and higher metal dispersion, thus the catalyst is less prone to deactivation. This discovery will help improve catalyst design.

In conclusion, waste-derived SiO₂ used as a catalyst support in the biogas dry reforming process shows a high catalytic activity and good stability, which is competitive with commercial and mesoporous ones. Considering the large-scale production and poor treatment conditions of photovoltaic waste SiCl₄, the production of waste-derived SiO₂ as well as its further application as a catalyst support for biogas dry reforming represents a useful conversion of photovoltaic waste to a high value-added product; it also provides a cheap and environmentally benign support for catalysts in the biogas dry reforming process.

Acknowledgements

The authors gratefully acknowledge the Hi-Tech Research and Development Program (863) of China for financial support (grant no. 20121868156).

References

- W. M. Budzianowski, Negative carbon intensity of renewable energy technologies involving biomass or carbon dioxide as inputs, *Renewable Sustainable Energy Rev.*, 2012, **16**(9), 6507–6521.
- S. Corthals, J. Van Nederkassel, H. De Winne, J. Geboers, P. Jacobs and B. Sels, Design of active and stable NiCeO₂ZrO₂MgAl₂O₄ dry reforming catalysts, *Appl. Catal., B*, 2011, **105**(3–4), 263–275.
- J. L. Ewbank, L. Kovarik, C. C. Kenvin and C. Sievers, Effect of preparation methods on the performance of Co/Al₂O₃ catalysts for dry reforming of methane, *Green Chem.*, 2014, **16**(2), 885.
- M. Broda, V. Manovic, Q. Imtiaz, A. M. Kierzkowska, E. J. Anthony and C. R. Muller, High-purity hydrogen via the sorption-enhanced steam methane reforming reaction over a synthetic CaO-based sorbent and a Ni catalyst, *Environ. Sci. Technol.*, 2013, **47**(11), 6007–6014.
- S. Chaemchuen, N. A. Kabir, K. Zhou and F. Verpoort, Metal-organic frameworks for upgrading biogas via CO₂ adsorption to biogas green energy, *Chem. Soc. Rev.*, 2013, **42**(24), 9304–9332.
- Y. Kathiraser, Z. Wang and S. Kawi, Oxidative CO₂ reforming of methane in La_{0.6}Sr_{0.4}Co_{0.8}Ga_{0.2}O₃-delta (LSCG) hollow fiber membrane reactor, *Environ. Sci. Technol.*, 2013, **47**(24), 14510–14517.
- A. Serrano-Lotina and L. Daza, Influence of the operating parameters over dry reforming of methane to syngas, *Int. J. Hydrogen Energy*, 2014, **39**(8), 4089–4094.
- V. M. Shinde and G. Madras, Catalytic performance of highly dispersed Ni/TiO₂ for dry and steam reforming of methane, *RSC Adv.*, 2014, **4**(10), 4817.
- A. Serrano-Lotina and L. Daza, Highly stable and active catalyst for hydrogen production from biogas, *J. Power Sources*, 2013, **238**, 81–86.
- Y. H. Taufiq-Yap, Sudarno, U. Rashid and Z. Zainal, CeO₂-SiO₂ supported nickel catalysts for dry reforming of methane toward syngas production, *Appl. Catal., A*, 2013, **468**, 359–369.
- A. R. Derk, G. M. Moore, S. Sharma, E. W. McFarland and H. Metiu, Catalytic Dry Reforming of Methane on Ruthenium-Doped Ceria and Ruthenium Supported on Ceria, *Top. Catal.*, 2013, **57**(1–4), 118–124.
- P. Frontera, A. Macario, A. Aloise, P. L. Antonucci, G. Giordano and J. B. Nagy, Effect of support surface on methane dry-reforming catalyst preparation, *Catal. Today*, 2013, **218–219**, 18–29.
- A. Luengnaruemitchai and A. Kaengsilalai, Activity of different zeolite-supported Ni catalysts for methane reforming with carbon dioxide, *Chem. Eng. J.*, 2008, **144**(1), 96–102.
- H. Y. Kim, J. N. Park, G. Henkelman and J. M. Kim, Design of a highly nanodispersed Pd-MgO/SiO₂ composite catalyst with multifunctional activity for CH₄ reforming, *ChemSusChem*, 2012, **5**(8), 1474–1481.
- Z.-J. Zuo, C.-F. Shen, P.-J. Tan and W. Huang, Ni based on dual-support Mg-Al mixed oxides and SBA-15 catalysts for dry reforming of methane, *Catal. Commun.*, 2013, **41**, 132–135.
- J. Zhu, X. Peng, L. Yao, D. Tong and C. Hu, CO₂ reforming of methane over Mg-promoted Ni/SiO₂ catalysts: the influence of Mg precursors and impregnation sequences, *Catal. Sci. Technol.*, 2012, **2**(3), 529.
- J. Zhu, X. Peng, L. Yao, J. Shen, D. Tong and C. Hu, The promoting effect of La, Mg, Co and Zn on the activity and

- stability of Ni/SiO₂ catalyst for CO₂ reforming of methane, *Int. J. Hydrogen Energy*, 2011, **36**(12), 7094–7104.
- 18 N. Wang, X. Yu, Y. Wang, W. Chu and M. Liu, A comparison study on methane dry reforming with carbon dioxide over LaNiO₃ perovskite catalysts supported on mesoporous SBA-15, MCM-41 and silica carrier, *Catal. Today*, 2013, **212**, 98–107.
- 19 I. Rossetti, J. Lasso, V. Nichele, M. Signoretto, E. Finocchio, G. Ramis and A. Di Michele, Silica and zirconia supported catalysts for the low-temperature ethanol steam reforming, *Appl. Catal., B*, 2014, **150–151**, 257–267.
- 20 M. M. Danilova, Z. A. Fedorova, V. I. Zaikovskii, A. V. Porsin, V. A. Kirillov and T. A. Krieger, Porous nickel-based catalysts for combined steam and carbon dioxide reforming of methane, *Appl. Catal., B*, 2014, **147**, 858–863.
- 21 X. Zhang, N. Wang, Y. Xu, Y. Yin and S. Shang, A novel Ni–Mg–Al-LDHs/ γ -Al₂O₃ Catalyst Prepared by in-situ synthesis method for CO₂ reforming of CH₄, *Catal. Commun.*, 2014, **45**, 11–15.
- 22 P. Djinović, I. G. Osojnik Črnivec, B. Erjavec and A. Pintar, Influence of active metal loading and oxygen mobility on coke-free dry reforming of Ni–Co bimetallic catalysts, *Appl. Catal., B*, 2012, **125**, 259–270.
- 23 D. H. Kim, H. O. Seo, M.-G. Jeong and Y. D. Kim, Reactivity and Stability of Ni Nanoparticles Supported by Mesoporous SiO₂ and TiO₂/SiO₂ for CO₂ Reforming of CH₄, *Catal. Lett.*, 2013, **144**(1), 56–61.
- 24 A. Goepfert, S. Meth, G. K. S. Prakash and G. A. Olah, Nanostructured silica as a support for regenerable high-capacity organoamine-based CO₂ sorbents, *Energy Environ. Sci.*, 2010, **3**(12), 1949.
- 25 X. Chen, J. Jiang, F. Yan, S. Tian and K. Li, A novel low temperature vapor phase hydrolysis method for the production of nano-structured silica materials using silicon tetrachloride, *RSC Adv.*, 2014, **4**(17), 8703.
- 26 I. Rossetti, A. Gallo, V. Dal Santo, C. L. Bianchi, V. Nichele, M. Signoretto, E. Finocchio, G. Ramis and A. Di Michele, Nickel Catalysts Supported Over TiO₂, SiO₂ and ZrO₂ for the Steam Reforming of Glycerol, *ChemCatChem*, 2013, **5**(1), 294–306.
- 27 M. A. A. Aziz, A. A. Jalil, S. Triwahyono, R. R. Mukti, Y. H. Taufiq-Yap and M. R. Sazegar, Highly active Ni-promoted mesostructured silica nanoparticles for CO₂ methanation, *Appl. Catal., B*, 2014, **147**, 359–368.
- 28 M. Zhao, T. L. Church and A. T. Harris, SBA-15 supported Ni-Co bimetallic catalysts for enhanced hydrogen production during cellulose decomposition, *Appl. Catal., B*, 2011, **101**(3–4), 522–530.
- 29 X. Wang, L. Meng, F. Wu, Y. Jiang, L. Wang and X. Mu, Efficient conversion of microcrystalline cellulose to 1,2-alkanediols over supported Ni catalysts, *Green Chem.*, 2012, **14**(3), 758.
- 30 B. Saha, A. Khan, H. Ibrahim and R. Idem, Evaluating the performance of non-precious metal based catalysts for sulfur-tolerance during the dry reforming of biogas, *Fuel*, 2014, **120**, 202–217.
- 31 L. Qian, Z. Ma, Y. Ren, H. Shi, B. Yue, S. Feng, J. Shen and S. Xie, Investigation of La promotion mechanism on Ni/SBA-15 catalysts in CH₄ reforming with CO₂, *Fuel*, 2014, **122**, 47–53.
- 32 F. Pompeo, G. F. Santori and N. N. Nichio, Hydrogen production by glycerol steam reforming with Pt/SiO₂ and Ni/SiO₂ catalysts, *Catal. Today*, 2011, **172**(1), 183–188.
- 33 G. Wu, C. Zhang, S. Li, Z. Han, T. Wang, X. Ma and J. Gong, Hydrogen Production via Glycerol Steam Reforming over Ni/Al₂O₃: Influence of Nickel Precursors, *ACS Sustainable Chem. Eng.*, 2013, **1**(8), 1052–1062.
- 34 S. Appari, V. M. Janardhanan, R. Bauri, S. Jayanti and O. Deutschmann, A detailed kinetic model for biogas steam reforming on Ni and catalyst deactivation due to sulfur poisoning, *Appl. Catal., A*, 2014, **471**, 118–125.
- 35 F. Shi, Y. Li, Q. Zhang, H. Wang and N. J. Dudney, Preparation of Core/Shell Structured Rutile/Anatase Photocatalyst via Vapor Phase Hydrolysis and its Photocatalytic Degradation of Phenol and Methylene Blue, *J. Am. Ceram. Soc.*, 2012, **95**(6), 1927–1932.
- 36 S. Appari, V. M. Janardhanan, R. Bauri and S. Jayanti, Deactivation and regeneration of Ni catalyst during steam reforming of model biogas: An experimental investigation, *Int. J. Hydrogen Energy*, 2014, **39**(1), 297–304.
- 37 C. Wu and P. T. Williams, A Novel Nano-Ni/SiO₂ Catalyst for Hydrogen Production from Steam Reforming of Ethanol, *Environ. Sci. Technol.*, 2010, **44**, 5993–5998.